Indian Journal of Fibre & Textile Research
Vol. 51, March 2026, pp. 118-129
DOI: 10.56042/ijftr.v51i1.15271

Preparation and investigation of graphene nanoplatelets effect on the structural, thermal, and morphological properties of short flax fibres nanocomposites

Nouredine Bouzegzi[1], Hakim Gouigah[1], Ismail Daoud[1, a], Mohamed Kenane[1], Isabel Lasanta Carrasco[2], Amar Manseri[3] & Francisco Javier Perez[2]

[1]Laboratory of Science and Materials Engineering, University of Sciences and Technology Houari Boumediene, Bab Ezzouar 16111, Algiers, Algeria

[2]Research Group of Surface Engineering and Nanostructured Materials, N_910627, Universidad Complutense de Madrid, Facultad de CienciasQuímicas, E-28040, Madrid, Spain

[3]Research Center of Semi-Conductor Technology for Energy, CRTSE-02, Bd. Dr. Frantz Fanon, B.P. 140 Algiers, 7 Merveilles 16038, Algeria

Received 24 November 2024; revised received and accepted 25 November 2025

In this paper, short flax fibres-graphene nanoplatelets (SFF-GNPs) nanocomposites were prepared by the solution mixing process. Graphene nanoplatelets (GNPs) was added at different mass loading (1, 5, 25, 50, and 100 wt.%) with short flax fibres (SFF). Nanofillers like graphene improve interfacial adhesion, strengthening composites and enhancing their durability. Therefore, understanding interfacial phenomena is key to developing high-performance hybrid nanocomposites. Various spectroscopic, thermal and morphological analysis techniques were employed to investigatethe effect of graphene nanoplatelets on the short flax fibres-graphene nanoplatelets nanocomposites properties. FTIR confirmed the absence of any chemical interactions between graphene nanoplatelets and short flax fibres, indicating the physical attachment of graphene nanoplatelets to the fibre surface by mechanical interlocking.According to XRD results, graphene nanoplatelets were identified on the surface off lax fibres, forming astaked layer. However, beyond 25 wt.%, disordered stacked layers were observed. In addition, SEM observations indicated that graphene nanoplatelets were tightly attached to the fibre surface, forming laminated layers, resulting in improved thermal stability of the short flax fibres as a function of graphene nanoplatelets content due to the barrier effect, which delayed fibre degradation.

Keywords: Flaxfibre, Graphene nanoplatelets, Mechanical interlocking, Nanocomposites, Natural fibres

1 Introduction

Nowadays, the industrial field is considered a source of vast quantities of solid wastes, with serious degradability issue. It has always posed a major recycling challenge with attention on preserving and protecting the environment. In fact, this has become a worldwide concern at present. It requires moving towards better reassuring alternatives with an eco-friendly attribute and working constantly to diminish its damaging effect on the environment as a result of industrial development remnants[1]. As an eco-friendly material, natural fibres are considered an excellent solution to this ecological dilemma. This fact has prompted researchers and manufacturers alike to expand their use due to the multiple features and advantages, namely; biodegradability, affordable cost, and satisfactory mechanical properties[2,3], besides good thermal and acoustic properties[4]. In addition, the trend of widely using natural lignocellulosic fibres, such as flax, jute, and cotton, as a fibre-reinforced polymer (FRP) is progressively increasing in many sectors, including construction, military, aerospace, automotive, biomaterials, and packaging[5]. However, natural fibres cannot be free from drawbacks, such as elevated moisture absorption and hydrophilicity[6]. Notably, the latter is primarily due to the non-cellulosic compounds, responsible for the poor compatibility with the hydrophobic polymer matrix. To address this issue, chemical treatment, such as alkali treatment, can be an effective solution to improve interfacial interaction. This method involves eliminating some portions of lignin and hemicellulose, along with impurities and extractible matters, such as pectin and wax[7]. Thereby improving the overall properties of the fibres.

Flax is a bast fibre whose existence dates back hundreds of years and has a diverse area of use. As

[a]Corresponding author.
E-mail: ismail.daoud@usthb.edu.dz

stated in the UN Food and Agriculture Organization (FAO) statistics, the worldwide production of raw and retted flax fibres in 2022 exceeded 950 thousand tons. It is mainly composed of cellulose (60-81%) as the most abundant fraction, hemicellulose (14-20.6%), lignin (2-3%), pectin (1.8-5%), wax (1.5-1.7%), water (10%), and water-soluble (3.9%)[8]. Based on their good mechanical properties, flax fibres stand as a promising alternative to substitute synthetic fibres such as glass and carbon fibres. Consequently, their use has become widespread over time[9]. Previous studies have focusedon flax fibres and their composites[9,10]. For example, Baley *et al.*[10] have tested a single flax fibre with a nominal length of 10 mm. The reported results were 54.08 GPa, 1339 MPa, 3.27%. for Young's modulus, tensile strength, and elongation at break, respectively. In addition, hybridization with both natural[11] and synthetic fibres[12], has enhanced flax hybrid composite properties.

Recently, the application of nanomaterial additives has continued to increase in different fields. Thus, their use as nanofillers has attracted numerous researchers aiming to acquire better performance for polymeric-based composites[13]. Among these nanomaterials, graphene and its derivatives, including graphene oxide (GO) and reduced graphene oxide (rGO), are highly appreciated and have received much attention by reason of their distinct properties[14]. Graphene is a two-dimensional (2D) material with sp^2 hybridized carbon atoms arranged as a honeycomb lattice originating from graphite. It was isolated for the first time in 2004 by Novoselov *et al.*[15] from graphite using mechanical exfoliation via scotch tape method. Today, grapheme can be obtained through several methods, including liquid phase-thermal exfoliation, and chemical vapor deposition (CVD)[16]. Moreover, grapheme is classified based on the number of layers, namely single-layer, bilayer, few-layer, and multi-layer[17]. Some of its attractive properties are electron mobility (200.000 $cm^2v^{-1}s^{-1}$), thermal conductivity (5000 $Wm^{-1}K^{-1}$), breaking strength (42 Nm^{-1}), elastic modulus (0.25 TPa), specific surface area (2630 m^2g^{-1} for monolayer), and impermeability to multiple gases and chemical substances[18]. Additionally, graphene nanoplatelets (GNPs) are an array of graphene layers stacked on top of each other, with thicknesses ranging from 0.7 to 100 nanometers[19].

The effect of graphene and its derivatives onfibre-reinforced-polymer-based composites have garnered the attention of several studies[20,21]. For instance, Kamaraj *et al.*[22] investigated the incorporation of graphene with flax fabric-reinforced epoxy composites. The tensile and flexure strength results had significantly improved when 0.1 wt.% graphene was added by 61 and 71%, respectively. Furthermore, other research highlights the effects of graphene on the performance of polymer-based composites reinforced with both natural and synthetic fibres, as it can effectively improve matrix fibre interfacial adhesion[23,24]. In addition, the thickness and concentration of the incorporated graphene into composite materials are also key factors to consider. In this sense, the effect of the number of layers on the thermal conductivity of graphene-epoxy composites was studied by Shen *et al.*[25]. They reported that composites with graphene nanoplatelets (n > 10) exhibited higher thermal conductivity compared to those reinforced with monolayer or few-layer graphene at the same loading. Srivastava *et al.*[26] investigated the effects of graphene nanoplatelets content on the mechanical properties of glass fibre/epoxy multilayer composites. The flexural results showed a 29% improvement with the addition of only 0.25 wt%.

Generally, there are two main approaches for incorporating such nanofillers when preparing fibre-reinforced-polymer-based composites: dispersing the nanofillers into the matrix or coating nanofillers on to the fibre surface. The first involves dispersing the nanofillers throughout the polymer matrix before mixing with fibres. Here, both nanofillers and fibresserve as hybrid reinforcement. The second approach consists of applying nanofillers-based coating on to the fibre surface, followed by adding the obtained hybrid composite to the polymer matrix. Regarding the last one, a few studies have been documented and reported. Recently, Mendonça Neuba *et al.*[20] investigated the effects of 0.1 wt.% graphene oxide (GO) coating on seven-islands sedge (Cyperusmalaccensis) fibres. Compared to uncoated fibres, GO coating enhanced the thermal and structural properties. Boudjellal *et al.*[27] prepared Alfa fibres/graphene nanoplatelets bio-based hybrid material. The resulting hybrid composite fibre showed uniform graphene nanoplatelets deposition on the surface alfafibre with good thermal stability, expecting its potential for advanced applications. Lea Maneval *et al.*[28] reported up to four-order-of-magnitude increase in the electrical conductivity of graphene-coated cationized cotton, with a permanent enhancement effect, suggesting new perspectives for possible applications as smart materials. Nevertheless, most studies exploit only the effect of nanofiller.

Therefore, controlling composite composition, optimizing nanofiller mass loading, and understanding the interactions and the possible phenomena occurred at the interface fibre-nanofiller can be beneficial to extend the area of applications for such coated fibres and their composites.

In light of the above-mentioned considerations, the purpose of this work is to investigate the effect of graphene nanoplatelets (GNPs) as a linked material on the surface of short flax fibres (SFF), focusing on the structural, thermal, and morphological properties. Various nanocomposites were prepared and analyzed using different characterization techniques, including RAMAN, FTIR, XPS, XRD, TGA, DSC, SEM, and TEM. The results were evaluated to assess the impact of the graphene nanoplatelets (GNPs) mass loading and to clarify the mechanisms, especially at the fibre/nanofiller interphase. This can be of great significance and provide valuable complementary insight, contributing to the future potential applications of these surface-modified fibres.

2 Materials and Methods

2.1 Materials

Flax fibres were procured from SICOMIN (France). Graphene nanoplateletswere purchased from NANOGRAFI (Turkey) with the following specifications: 99.9% purity, average thickness of 3 nm, specific surface area of 320 m^2/g, and a diameter of 1.5 μm. Figure 1 displays TEM micrographs of GNPs at low and high magnification. As shown, a clear contrast in blackness degree is observed, resulting from the overlapping of the planer GNPs layers [Fig. 1(a)]. On the other hand, [Fig. 1(b)] illustrates a set of layers stacked on top of each other with a thickness of 4.32 nm, confirming the technical specifications provided by the manufacturer.

2.2 Preparation of Short Flax Fibres (SFF)

The flax fibres were manually chopped into short fibres with an average length of 3mm. Then, the obtained fibres were subjected to Soxhlet extraction for 6h using a solvent composed of toluene-ethanol (62/38%, (v/v)), followed by dryingat 70°C for 6h.

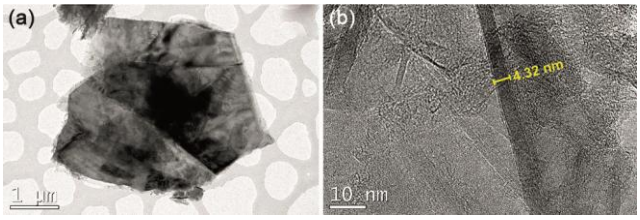

Fig. 1 — TEM micrographs of GNPs at (a) low magnification and (b) high magnification

2.3 Alkali Treatment

To remove the amorphous non-cellulosic components and impurities, alkali treatment was applied. The fibres were immersed in a glass containerusing NaOH solution at 10s % for 3h. A chemical reaction occurs between the hydroxyl group of short flax fibresand sodium hydroxide solution compounds, according to the following equation:

$$\text{Fibre} - \text{OH} + \text{NaOH} \rightarrow \text{Fibre} - \text{O} - \text{Na} + \text{H}_2\text{O} \quad \ldots (1)$$

Afterward, the fibres were washed profusely using distilled water. Then, a neutralization process was done using acetic acid (CH_3COOH) until reaching a neutral pH. Finally, adry-up operation was necessary at 70°C for 24h.

2.4 CompositesPreparation (SFF-GNPs)

Initially, GNPs were dispersed into ethanol at a concentration of 1 mg/mL, followed by a sonication for 2 h. Subsequently, different nanocomposites were prepared using various percentages of the dispersed GNPs (1, 5, 25, 50, and 100 wt.%) relative to the fixed weight of the fibres by a simple solution mixing method. For example, to prepare SFF-25%GNPs nanocomposite containing 1g of SFF, a quantity of 0.25 g of GNPs is required, which is equivalent to 250 mL of dispersed GNPs solution. Then, the mixture was magnetically stirred at 300 rpm for 2 h at 70 °C. Finally, SFF-GNPs nanocomposite was dried at 70 °C for 6 h to eliminate the residual ethanol. Table 1 summarizes the formulations of the prepared SFF-GNPs nanocomposites. The schematic presentation of nanocomposite preparation steps by solution mixing method is displayed in Fig. 2. The obtained SFF-GNPs nanocomposites with varying GNPs content are illustrated in Fig. 3. It is clearly observed that the level of blackness contrast increases as a function of GNPs content, reflecting the quantity of GNPs attached on the flax surface.

Table 1 — Formulation of the prepared SFF-GNPs nanocomposites

Designation	Formulation	GNPs (wt.%)
Graphene Nanoplatelets	GNPs	-
Short Flax Fibres	SFF	0
SFF-GNPs nanocomposite	SFF-1%GNPs	1
	SFF-5%GNPs	5
	SFF-25%GNPs	25
	SFF-50%GNPs	50
	SFF-100%GNPs	100

2.5 Testing Methods

A range of characterization methods were used to investigate the structural, thermal, and morphological characteristics of GNPs, SFF, and SFF-GNPs nanocomposites, detailed as follows: Raman spectroscopy analysis was assessed using a RENISHAW Spectrometer at room temperature. An operating power of 25 mW and a 633 nm laser excitation were used. The spectra were plotted between 500 and 3500 cm^{-1}. Fourier Transform Infrared Spectroscopy Analysis (FTIR) was conducted using a Jasco FT/IR-4X Spectrometer. The scan was taken between 4000-400 cm^{-1}, with a resolution of 4 cm^{-1}. The mean values were taken from 64 scans for each sample. The X-ray photoelectron spectroscopy (XPS) was analyzed using an XPS ESCALAB 250XI Spectrometer (Thermo Fisher Scientific Inc, MA, USA), with a monochromatic Al-Kα radiation source at emission energy of 1486.6 eV. The peaks deconvolution of survey data was analyzed using Casa XPS 2.3.25. Thermogravimetric analysis (TGA) was accomplished using an SDT Q600 instrument from TA Instruments at a heating rate of 10°C/min, from 50°C to 500°C under a nitrogen environment. Differential Scanning Calorimetry Analysis (DSC) was recorded under a nitrogen gas atmosphere using a Q20 instrument from TA Instruments. The temperature ranges from 20°C to 400°C with 10°C/min asa heating rate.X-ray diffraction (XRD) measurements were carried out, based on Bragg's equation ($n\lambda = 2d \sin\theta$), using PAN alytical X-pert PRO MRD diffractometer, equipped with aCuKα radiation at λ = 1.54060 Å. The scan was operated at 40 kV/15 mA, and 2θ sweeps from 10°to 70° with a step size of 0.03°. Scanning electron microscopy analysis (SEM) was performed using JEOL JSM-7610F Plus (JEOL Ltd., Tokyo, Japan) with Schottky-type field emission (S-FEG). Transmission electron microscopy (TEM) was achieved using a JEOL JEM 2100 instrument operated with a LaB6 electron gun at 200 kV (JEOL Ltd., Tokyo, Japan) equipped with a CCD camera (Orious SC1000).

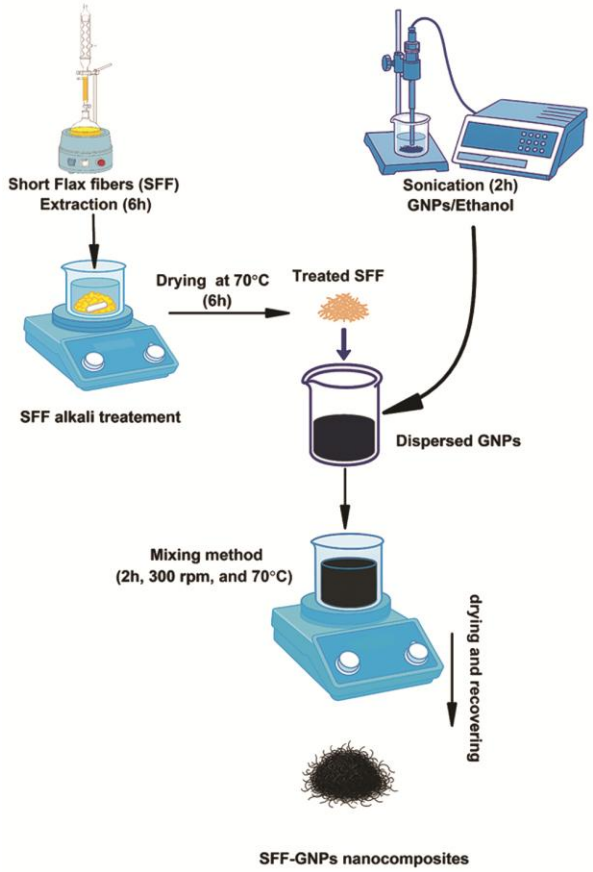

Fig. 2 — Schematic illustration of SFF-GNPs nanocomposites preparation steps

3 Results and Discussion

3.1 RAMAN Spectroscopy

Raman spectra of SFF, GNPs, and SFF-GNPs nanocomposites are shown in Fig. 4. From an initial inspection of the curves, it is evident that there is an almost complete similarity among the various SFF-GNPs nanocomposites when compared to GNPs, except for the SFF-1% GNPs nanocomposite. The presence of the D peak appearing at ~1330 cm^{-1} reveals the defects and disorder in the structure of GNPs[29]. The G band with a peak at ~1580 cm^{-1} in GNPs and SFF-GNPs nanocomposites is due to the

Fig. 3 — Images of SFF and SFF-GNPs nanocomposites

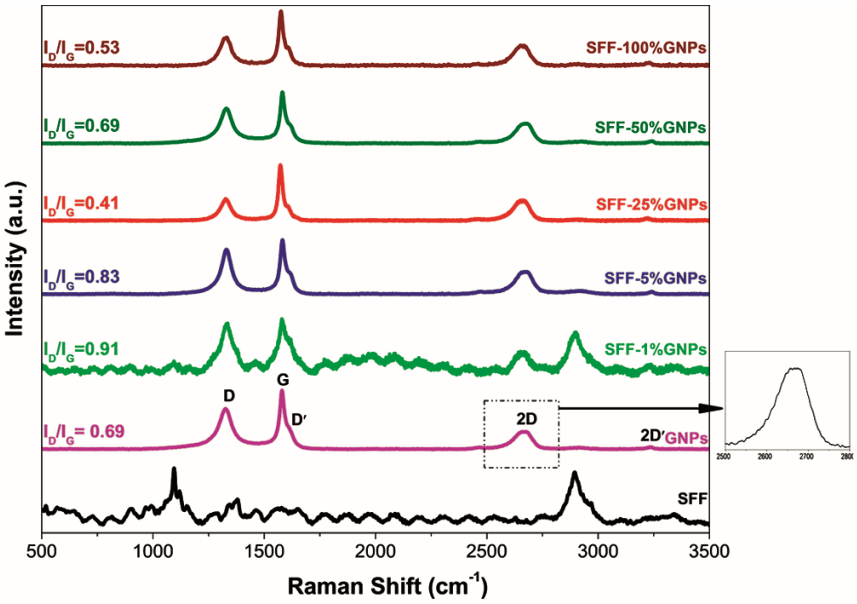

Fig. 4 — RAMAN spectra of SFF, GNPs, and SFF-GNPs nanocomposites

sp^2 hybridization of carbon atoms. This hybridization is related to the in-plane vibrational mode after C-C bonds excitation[30]. Moreover, it can be observed that GNPs and SFF-GNPs nanocomposites present a slight shoulder D′ peak at ~1615 cm^{-1}, which is attributed to defects too. Moreover, the splitting of the 2D band at ~2670 cm^{-1}, originating from the phonon branches or electronic bands, confirms the presence of graphene in nanoplatelets from. Additionally, The shift of this 2D band towards 2670 cm^{-1}can be referred to the graphene containing more than 10 layers, which is characteristic of graphene nanoplatelets[31]. Furthermore, the 2D band for SFF-GNPs nanocomposites remains nearly unchanged, meaning GNPs layers were neither affected nor changed. The small 2D′ peak at ~3230 cm^{-1} is present in the Raman spectrum of GNPs, does not necessarily reflect the presence of defects. It is also considered the second-order mode of the D′ peak[30]. However, a new peak appears at 2901 cm^{-1} in the SFF-1% GNPs nanocomposite, distinguishing it from other SFF-GNPs nanocomposites, originating from cellulose structure in flax fibres[32]. In addition to this peak in flax fibre, another salient peak at ~1096 can be observed due to the stretching vibration of asymmetric C-O-C ring[33]. Moreover, the appearance of the characteristic peaks of GNPs in SFF-1% GNPs confirms their existence on the flax surface.

The D-band and G-band intensity ratios (I_D/I_G) of GNPs and SFF-GNPs nanocomposites were calculated to estimatethe level of disorder or defects

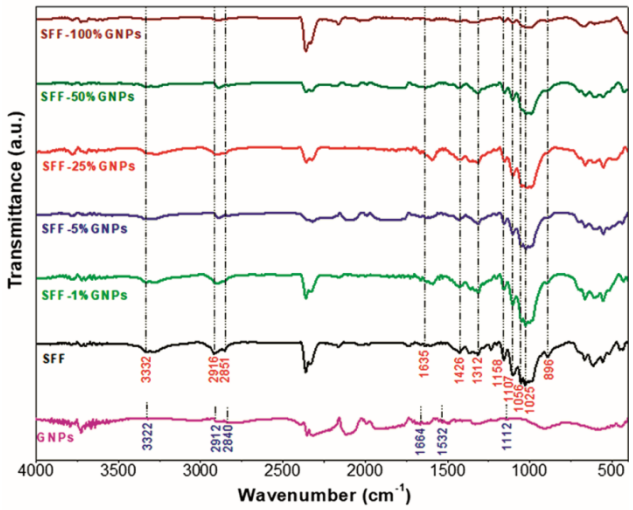

Fig. 5 — FTIR spectra of GNPs, SFF, and SFF-GNPs nanocomposites

present. The I_D/I_G ratio was found 0.69 for GNPs, which is close to the value reported by Iván *et al.*[34]. The obtained I_D/I_G results for SFF-1%GNPs, SFF-5% GNPs, SFF-25%GNPs, SFF-50%GNPs, and SFF-100% GNPs were 0.91, 0.83, 0.41, 0.69, and 0.53, respectively. Notably, at low GNPs content (1 and 5%), the I_D/I_G ratio increases, then it tends to decrease for the high GNPs content. The result can be linked to the reduction of sp^2 clusters [27].

3.2 Fourier Transform Infrared Spectroscopy (FTIR)

The possible chemical interactions between the flax fibres and the graphene nanoplatelets were investigated through the FTIR technique. Figure 5

shows the FTIR spectra of SFF, GNPs, and SFF-GNPs nanocomposites. The GNPs spectrum displays the presence of a weak peak around 3322 cm^{-1}, corresponding to the -OH stretching vibration of the hydroxyl groups. As expected, the peak corresponding to the aromatic C=C was observed at around 1532 cm^{-1}, reflecting the skeletal vibrations of the graphitic backbone from the hexagonal structure[35]. In addition, two peaks were identified at around 2840 cm^{-1} and 2912 cm^{-1}, related to the C-H stretching vibrations. Moreover, the characteristic peaks at 1664 cm^{-1} and 1112 cm^{-1} were due to C-C and C-O stretching vibrations, respectively. The appearance of the oxidized or hydroxyl groupsin GNPs is likely related to the effect of oxidation during the purification process or atmospheric moisture.

In the SFF spectrum, the absorption band at 3332 cm^{-1} is attributed to the stretching vibration of hydroxyl groups O-H present in the crystalline structure of cellulose. However, the absence of the peak at 1735 cm^{-1}, typically associated with natural fibres, indicates the successful removal of certain components through the alkali treatment. The peaks positioned at 2916 cm^{-1} and 2852 cm^{-1} correspond to the stretching vibration of C-H and CH_2 functional groups found in cellulose and hemicellulose. Additionally, the peak at 1635 cm^{-1} is ascribed to the O-H bending vibration of adsorbed water in the fibre. The peaks around 1426 $cm^{-1}$and 1312 $cm^{-1}$are associated with the CH_2 asymmetric bending in cellulose. Moreover, the C-C and C-O-C stretching vibrations, assigned to the ring breathing of polysaccharides in cellulose, appear at the positions 1158 cm^{-1} and 1107cm^{-1}, respectively. The absorption peaks at 1056 cm^{-1} and 1025 cm^{-1} are attributed to the C-OH stretching vibrations of cellulose, while the peak at 896 cm^{-1} corresponds to the bending vibration of C-H. The characteristic bands of SFF and SFF-GNPs nanocomposites are nearly identical, indicating that there is no chemical interaction between SFF and GNPs. This implies that the GNPs are likely mechanically interlocked to the SFF surface. However, a notable difference in peak intensity is observed in the SFF-GNPs nanocomposites related to the GNPs content. The presence of GNPs on the fibre surface leads to a decrease in the intensities of the different bands. Thus, as the GNPs content increases, a smaller number of bonds are detected. This behavior was also observed in Ouadil *et al.*[36] work regarding knit polyester fabric-graphene composites.

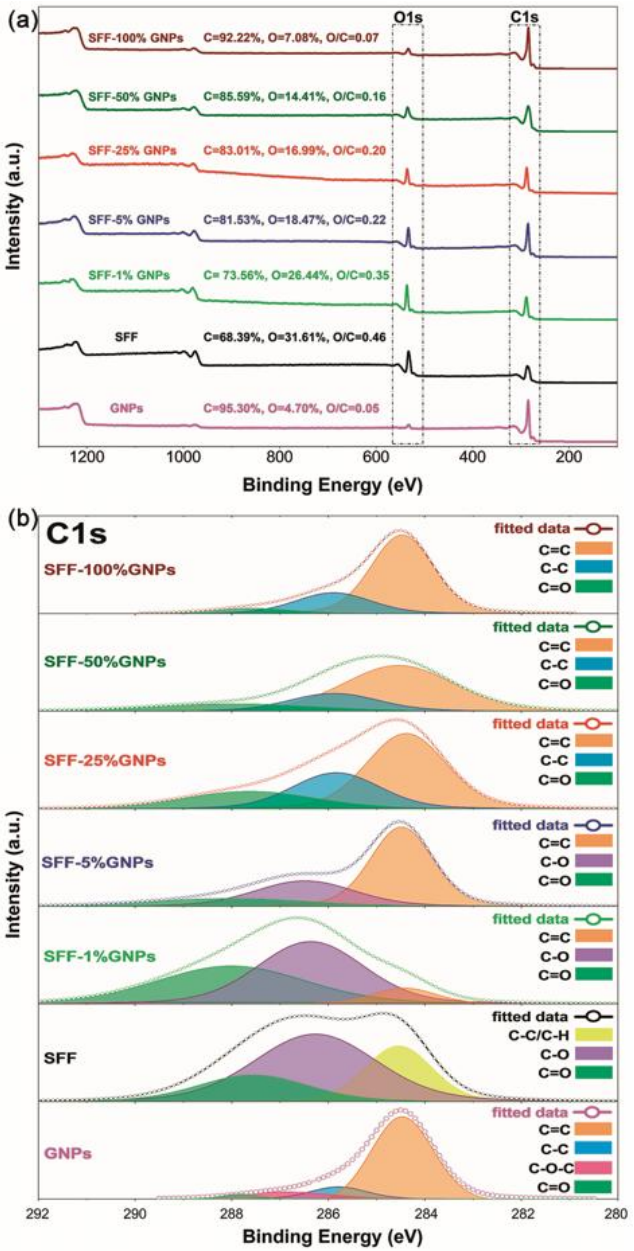

Fig. 6 — XPS measurements of GNPs, SFF, and SFF/GNPs nanocomposites (a) survey XPS spectra and (b) high-resolution C1s XPS spectra

3.3 X-ray Photoelectron Spectroscopy (XPS)

The surface of the SFF-GNPs nanocomposites was analyzed using XPS technique to identify their chemical composition and the functional groups present. Figure 6 shows the XPS survey and the deconvolution of high-resolution C1s spectra of GNPs, SFF, and SFF-GNPs nanocomposites. As shown in survey spectra [Fig. 6(a)], all analyzed nanocomposites exhibit the presence of two peaks

corresponding to the binding energy of carbon (C1s) and oxygen (O1s) at 284 eV and 532 eV, respectively. GNPs present a high carbon content of 95.30% and a low oxygen content of 4.7%, giving an O/C ratio of 0.05. The existence of oxygen is attributed to the oxidized carbon at the edges of individual graphene planes and its distribution on the basal planes. The oxygen content can vary depending on the GNPs characteristics, such as the specific surface area, number of layers, and particle size. Blurton *et al*.[37] reported an oxygen content of 6.8 at.% for GNP with an average particle size of 10 μm and surface area of 22.83 m^2/g. They estimated that approximately 0.01-0.06% of all oxygen atoms are located at the edges of individual graphene flakes. Hence, the high obtained content indicates that the oxygen is distributed not only along the flake edges but also throughout the basal planes of the graphene nanoplatelets. On the other hand, SFF has an elementary composition of approximately 68 (% in carbon atoms and 32% in oxygen atoms, resulting in an O/C ratio of 0.46. In comparison, untreated flax fibreshave an O/C = 0.15[38], indicating that the O/C ratio increases after alkali treatment. It is worth mentioning that flax fibre surface treatment using various methods, such as alkali treatment, can raise the O/C ratio. The increase after alkali treatment is attributed to the combination effects of wax removal and hydrogen bonds breaking, which increases the cellulose abundance on the flax fibre surface. As for SFF-GNPs nanocomposites, the percentage change in the measured atomic fraction of O and C reveals a decrease in the O/C ratio as a function of GNPs content. The higher GNPs added, the lower the O/C ratio is obtained. This decline confirms the increasing amount of GNPs attached to the flax fibre surface.

Fig. 6(b) shows the high-resolution of the C1s region. Additionally, the corresponding bonds are summarized in Table 2. In the case of GNPs, the deconvolution of C1s photoelectronspectrum revealed three different functional groups for carbon: a prominent peak forC=C sp^2 at 284.47 eV, a second peak forC-C sp^3at 285.78 eV, and two small peaks for oxygen containing bonds, C-O-C and C=O, at 286.89 eV and 287.90 eV, respectively. The identified bonds areconsistent with those published for graphene[39]. Moreover, the intensity of the C=C bond is higher than that of the C-C bond, indicating the presence of defects, which is consistent with the Raman findings. Regarding SFF, the fitted peaks at 284.53, 286.26, and 287.55 eV were assigned to C-C/C-H, C-O, and C=O bonds, respectively. The C-C/C-H bond is associated with aliphatic carbons originating from cellulose and hemicelluloses, as well as the aromatic structures of lignin. The second peak at 286.26 eV describes the carbon-oxygen single bond, denoted by C-O, referring to the hydroxyl groups and ether bonds in cellulose and lignin, respectively. The last peak at 287.55 eV corresponds to C=O bond, attributed to the carbonyl functional group associated with the cellulose compound. These bonds align with those described in the literature for flax fibres[38]. From the decomposition of the C1s spectrum of SFF-GNPs nanocomposites, a significant change is observed in the C=C bond peak at 284 eV, showing a notable increase as a function of GNPs content. As more GNPs are added, the progressive rise in the C=C peak intensity indicates a greater degree of carbon-carbon double bonds on the flax fibre surface. This could be indicative of mechanical interlocking between the SFF and the GNPs. Furthermore, up to 5% GNPs, the C-O bond remains around 286 eV, originating from flax fibre. However, starting from 25% GNPs, the C-C bond originating from GNPs appears around 285.8 eV, while the C-O bond disappears. Thus, the addition of GNPs results in the emergence of the C-C bond, as GNPs are composed almost entirely of carbon atoms, confirming their coverage on the fibre surface followed by the formation of stacked layers of

Table 2 — Functional groups obtained from the deconvoluted high-resolution C1s spectra

Functional group	C-C/C-H	C-O	C=O	C=C	C-C	C-O-C
	Binding Energy (eV)					
GNPs	-	-	287.90	284.47	285.78	286.89
SFF	284.53	286.26	287.55	-	-	-
SFF-1% GNPs	-	286.36	288.62	284.48	-	-
SFF-5% GNPs	-	286.45	288.03	284.48	-	-
SFF-25% GNPs	-	-	287.62	284.40	285.83	-
SFF-50% GNPs	-	-	287.92	284.54	285.87	-
SFF-100% GNPs	-	-	287.56	284.40	285.89	-

GNPs. This finding is supported previously by the decrease in the O/C ratio with the increase in GNPs content.

3.4 X-Ray DiffractionAnalysis (XRD)

The XRD patterns of GNPs, SFF, and SFF-GNPs nanocomposites are given in Fig. 7. SFF exhibits two slight diffraction peaks at 2θ = 14.67° and 16.45°, referred to lignin and hemicelluloses, along with a prominent peak at 22.66° associated with the typical plan diffraction of cellulose. These three peaks correspond to the (101), (10$\bar{1}$), and (002) planes, respectively.

On the other hand, the GNPs diffraction appears at 2θ = 26.38° with a sharp graphitic plane peak (002), which is related to the interlayer d-spacing of 3.4 Å. Besides, a set of small peaks at 2θ = 42.22°, 44.39°, and 54.54° can be assigned to the graphitic plane reflections (100), (101), and (004), respectively. Concerning the SFF-GNPs nanocomposites, the XRD patterns are nearly identical, with no new peaks observed, indicating no interaction between the GNPs and the flax fibres. Therefore, the XRD patterns reflect a combination of the characteristic peaks from both SFF and GNPs materials. However, A remarkable increase is observed in (002) GNPs peak intensity as a function of the GNPs content. This variation can be related to stacking and agglomeration phenomena[40]. Moreover, this increase indicates a rise in plan-to-plan contact, resulting in a uniform distribution of GNPs. Consequently, more GNPs can stack on the fibre surface. These findings are in good agreement with the results previously highlighted in FTIR and XPS analyses. While, a broadening for the (002) peak occurs beyond 25% of GNPs which can be attributed to the disorder of the stacked GNPs[41].

3.5 ThermogravimetricAnalysis (TGA) and Derivative Thermogravimetry (DTG)

The evolution of TGA and DTG curves of GNPs, SFF, and SFF-GNPs nanocomposites are presented in Fig. 8. As seen in Fig. 8 (a), unlike GNPs, which exhibit a stable thermal behaviour with a total mass loss of 3.5%, all other samples depict a similar decomposition profile, with different mass loss and residual weight percentages. Importantly, the decomposition of SFF and SFF-GNPs nanocomposites occurs in three distinct phases: phase I (50–220°C), phase II (220–430°C), and phase III (430–500°C). In phase I, aslight weight loss is observed, which can be subdivided into two parts. The first part, up to 100°C, is related to the evaporation of the moisture within the fibre. The second part, extending to 220°C, is mainly associated with the decomposition of hemicellulose. By the end of this phase, the final mass loss ranges from approximately1 to 4%. The next phase is considered

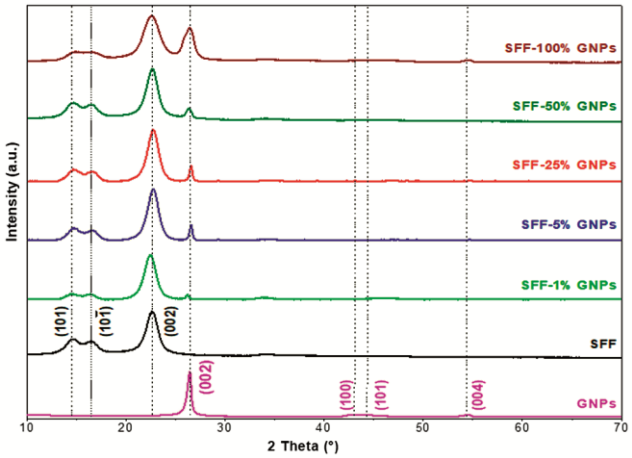

Fig. 7 — X-Ray diffractograms of GNPs, SFF, and SFF-GNPs nanocomposites

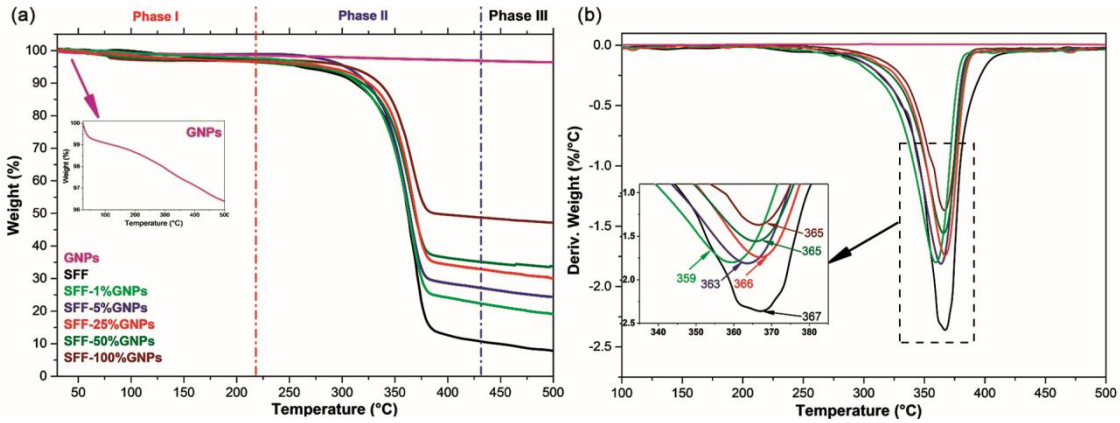

Fig. 8 — (a) TGA and (b) DTG curves of GNPs, SFF, and SFF-GNPs nanocomposites

the most important stage of the thermal decomposition process, where significant degradation takes place, primarily due to the decomposition of the cellulose component. Table 3 summarizes the calculated degradation temperatures (T_{onset} and T_{max}) and the weight loss percentage obtained from the TGA and DTG curves. Here the T_{onset} values were determined using the two tangents inter section method. It is clearly observed that the T_{onset} of SFF is lower than that of the other SFF-GNPs nanocompositesin the order of13-23°C, which is related to the increase in GNPs quantity. A similar decrease is also noted in weight loss. At the end of this phase, the maximum degradation reaches 89.5% for graphene-free fibres SFF, whereas the lowest degradation, for SFF-100% GNPs nanocomposite, attained 51.3%. At the same time, the DTG curves exhibited a pronounced degradation rate during this phase, which corresponds to the cellulose depolymerization[42].With further GNPs addition, the DTG curves shift toward lower temperatures (T_{max} magnified in Fig. 8(b)). Meanwhile, a decrease in the degradation rate is observed. Hence, the higher the GNPs content, the lower the fibre degradation rate is obtained. The final phase (430-500°C) exhibits a slow decomposition with variable ash residue rates, resulting from the decomposition of SFF at the end of this thermal degradation process. The weight loss decreases from 80.9% for SFF-1% GNPs to 52.9% for SFF-100% GNPs, reflecting an improvement ranging from 11.9% to 42.4%, depending on the GNPs content (from 1 to 100%) relative to the SFF, which reaches a total weight loss of 91.9%. In this phase, the decomposition is due to the degradation of cellulose and lignin. However, lignin is known as the most thermally-resistant component and exhibits a wide range of degradation temperatures (from 180 to 500°C) due to its complex aromatic structure. In summary, as depicted in the TGA and DTG curves, increasing GNPs content significantly enhances the thermal stability and resistance to thermal degradation of nanocomposites compared to SFF. This improvement can be attributed to the barrier effect created by GNPs, which enhances the ability to delay the thermal decomposition of the SFF[23].

3.6 Differential Scanning Calorimetry (DSC)

The DSC curves of GNPs, SFF, and SFF-GNPs nanocomposites are shown in Fig. 9. A broad endothermic peak is detected in the range of 104–173°C, with a related enthalpy corresponding to the maximum energy required for the evaporation of the retained moisture from SFF and SFF-GNPs nanocomposites. Similarly, the endothermic transition for GNPs was observed at around 128°C. Notably, the addition of GNPs increases both the temperature and the required enthalpy for all the nanocomposites. In addition, SFF and SFF-GNPs nanocomposites displayed a second endothermic peak, ranging from 354 °C to 368°C (as indicated by the dashed rectangle). This peak deals with the corresponding

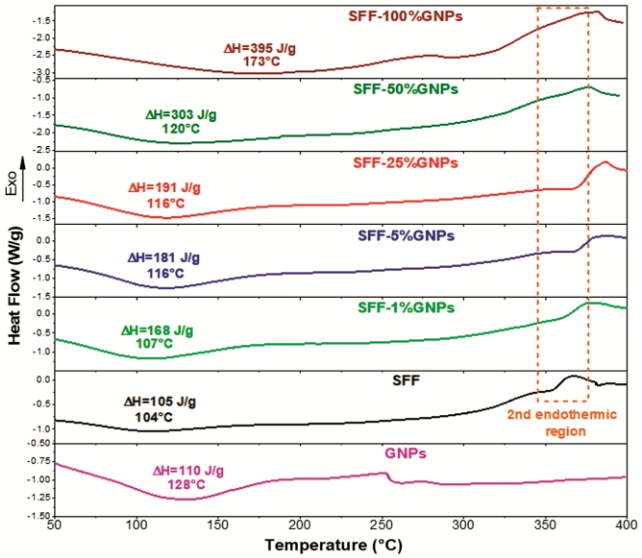

Fig. 9 — DSC thermosgrams of GNPs, SFF, and SFF-GNPs nanocomposites

Table 3 — Degradation temperatures and weight loss of GNPs, SFF, and SFF-GNPs nanocomposites

Sample	T_{onset}, °C	T_{max}, °C DTG peak	Weight loss, % (Phase I+II)	Residue at 500 °C, % (Phase III)
GNPs	-	-	3.1	96.5
SFF	324	367	89.5	8.1
SFF-1% GNPs	337	359	77.7	19.1
SFF-5% GNPs	338	363	72.9	24.2
SFF-25% GNPs	341	366	67.2	29.8
SFF-50% GNPs	343	365	64.9	33.6
SFF-100% GNPs	347	365	51.3	47.1

peak observed in the DTG curves, suggesting the degradation of fibre components such as cellulose and lignin at this temperature. However, a decrease in the enthalpies required for the decomposition is observed with increasing graphene content, which supports the hypothesis that thermal stability is enhanced due to the barrier effect of graphene. Kim and Lee[43] reporteda similar trend for the electrical heating textile coated with high content of graphene nanoplatelets/polyvinylidene fluoride-co-hexafluoropropylene (GNP/PVDF-HFP)composite.

3.7 Morphological Analysis

SEM analysis can provide information about the interlocking, interfacial adhesion, and dispersion state of the GNPs on the fibre surface. The SEM micrographs of SFF, GNPs, and SFF–GNPs nanocomposites are depicted in Figs. 10 and 11.

Figs. 10 (a, b) clearly illustrate the morphology of GNPs with different sizes. The comparison between untreated and treated fibre reveals that the raw fibre exhibits a rough surface with the presence of distinguishable impurities, attributed to non-cellulosic compounds such as hemicellulose, lignin, and waxes (Figs. 10 b, c). While, after alkali treatment, the flax fibre surface appears rough and irregular but much cleaner due to the removal of non-cellulosic constituents, as indicated in Figs. 10 (e, f). By way of example, EDS mapping of the treated fibre shows the uniform distribution of the key chemical elements (carbon and oxygen) across the entire fibre.

For the SFF–GNP nanocomposites, Fig. 11 illustrates the surface state of the SFF fibres with

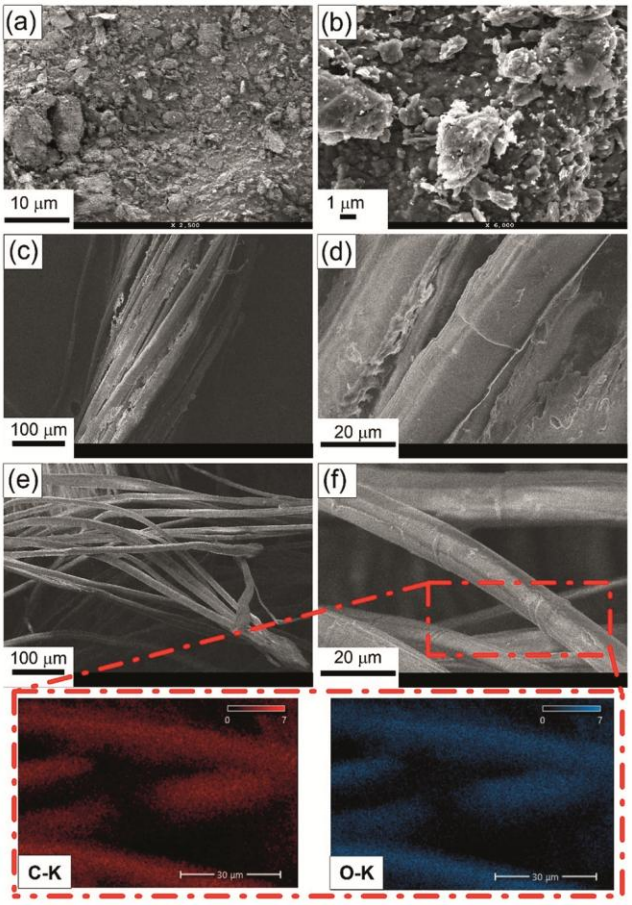

Fig. 10 — SEM micrographs of (a, b) GNPs, (c, d) untreated SFF, (e, f) treated SFF, and the corresponding elemental composition maps of C and O

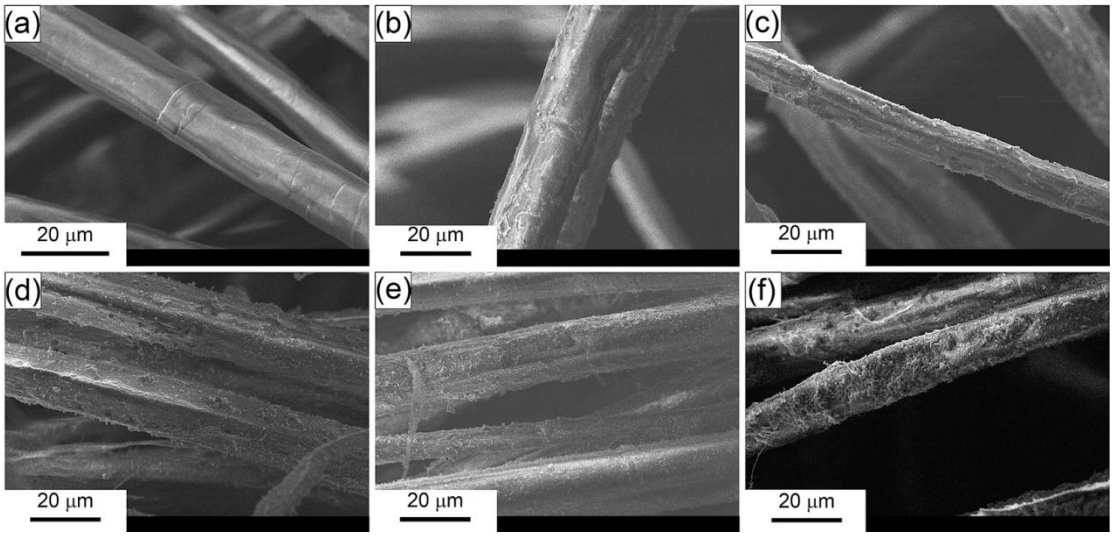

Fig. 11 — SEM micrographs of (a) treated SFF and SFF-GNPs nanocomposites with GNPs mass loading of (b) 1%, (c) 5%, (d) 25%, (e) 50%, and (f) 100%.

different GNPs mass loading. As the GNPs loading increases, a greater quantity is attached to the SFF surface. On the other hand, independent of the GNPs percentage, it is evident that GNPs are firmly attached to the SFF surface. However, at higher loadings, the GNPs cover the entire external surface and form laminated layers. The GNPs tend to form stacked clusters resulting from π–π and van der Waals interactions between the nanoplatelet layers[44]. These findings align with the XRD results, which indicate the formation of stacked layers on the fibre surface. Similar results were reported by Boudjellal *et al*.[27] for Alfa fibre/GNPs hybrid composites, where stratification was attributed to the good adhesion of GNPs on the surface of the natural Alfa fibres. In another study, Saker *et al*.[45] reported a better mechanical interlocking of graphene on the jute fibre surface due to its diffusion onto the rough and porous treated surface.

4 Conclusion

Short flax fibres-graphene nanoplatelets (SFF-GNPs) nanocomposites were successfully prepared by mixing solution method. The effect of GNPs on structural, thermal, and morphological properties of SFF-GNPs nanocomposites was investigated at various GNPs mass loading. The TEM images display overlapping layers, confirming the graphene classificationas nanoplatelets. This was further confirmed by the splitting observed in the 2D peak in Raman analysis. The FTIR analysis confirms the absence of any chemical interaction between SFF and GNPs, suggesting the mechanical interlocking hypothesis. Based on XPS analysis, the O/C ratio decreases with increasing GNPs content, indicating a greater degree of carbon-carbon bonds and surface coverage. These results are corroborated by the SEM micrographs. Additionally, SEM revealed that GNPs were stacked on the surface of the flax fibres, forming laminate layers. According to XRD results, GNPs were identified on the surface of flax fibres. However, beyond 25 wt.%, a broadening of the (002) peak of GNPs is observed, which can be attributed to the disorder in the stacked layers. The TGA analysis results demonstrated a significant improvement in the thermal stability of SFF as a function of GNPs content. The lower degradation was observed for SFF-100% GNPs, delaying the T_{Onset} by 23 ℃ and reducing the degradation rate by 42.4% compared to SFF, highlighting the positive effect of GNPs. These findings were further endorsed by DSC analysis. Furthermore, DSC curves indicated the presence of two endothermic peaks related to moisture evaporation and fibre degradation. In summary, the outcomes suggest that incorporating GNPs with flax fibres can offer potential benefits for developing high-performance hybrid-basednanocomposites. This paper mayserve as a valuable complement to ongoing research on natural fibres.

Acknowledgements

The authors gratefully acknowledge the technical support of MT Miguel Gamo and Noemi Encinas Garcia from the Universidad Complutense de Madrid for their assistance.

References

1 Hamada H M, Shi J, Abed F, Al Jawahery M S, Majdi A & Yousif S T, *Sci Total Environ*, 876 (2023) 162804.
2 Lalit R, Mayank P & Ankur K, *J Mech Eng*, 68 (1) (2018) 33.
3 Suriani M J, Ilyas R A, Zuhri M Y M, Khalina A, Sultan M T H, Sapuan S M, Ruzaidi C M, Wan F N, Zulkifli F, Harussani MM, Azman M A, Radzi F S M & Sharma S, *Polymers*,13 (20) (2021).
4 Dev B, Rahman M A, Repon M R, Rahman M M, Haji A & Nawab Y, *Polym Compos*, 44 (11) (2023) 7235.
5 Kamarudin S H, Mohd Basri M S, Rayung M, Abu F, Ahmad S B, Norizan M N, Osman S, Sarifuddin N, Desa M S, Abdullah U H, Mohamed Amin Tawakkal I S & Abdullah L C, *Polymers*,14 (17) (2022) 3698.
6 Gholampour A & Ozbakkaloglu T, *J Mater Sci*, 55 (3) (2020) 829.
7 Jagadeesh P, Puttegowda M, Mavinkere Rangappa S & Siengchin S, *Polym Compos*, 42 (12) (2021) 6239.
8 Moudood A, Rahman A, Öchsner A, Islam M & Francucci G, *J Reinf Plast Compos*, 38 (7) (2018) 323.
9 More AP, *Adv Compos Hybrid Mater*, 5 (1) (2022) 1.
10 Baley C, *Compos Part A Appl Sci Manuf*, 33 (7) (2002) 939.
11 Rouibah H, Mohamed K & Ismail D, *Indian J Fibre Text Res*, 45 (4) (2021) 426.
12 Abd El-Baky M A, Attia M A, Abdelhaleem M M & Hassan M A, *J Nat Fibres*,19 (3) (2022) 954.
13 Sun J, Liu J, Sun X, Gao Z, Wang D, Jin Z & Gao H, *Adv Eng Mater*, 27 (10) (2025) 2402879.
14 Lee X J, Hiew B Y Z, Lai K C, Lee L Y, Gan S, Thangalazhy-Gopakumar S & Rigby S, *J Taiwan Inst Chem Eng*, 98 (2019) 163.
15 Novoselov K S, Geim A K, Morozov S V, Jiang D, Zhang Y, Dubonos S V, Grigorieva I V & Firsov A A, *Science*, 306 (5696) (2004) 666.
16 Novoselov K S, Colombo L, Gellert P, Schwab M & Kim K, *nature*, 490 (7419) (2012) 192.
17 Bianco A, Cheng H M, Enoki T, Gogotsi Y, Hurt R H, Koratkar N, Kyotani T, Monthioux M, Park CR, Tascon JMD& Zhang J, *Carbon*,65 (2013) 1.
18 Ghany N A A, Elsherif S A & Handal H T, *Surf Interfaces*, 9 (2017) 93.
19 Jiménez-Suárez A & Prolongo S G, *Appl Sci*, 10 (5) (2020) 1753.

20 de Mendonça Neuba L, Felipe Pereira Junio R, Silva D S, Palmeira A A, Tavares S, Lazarus B, Pereira A C & Monteiro S N, *J Nat Fibres*, 21 (1) (2024) 2392284.

21 Xu R, Xue Z, Yang D, Li X, Nie H, Guo Y, Guo H, Yan Q-L & Gu J, *Adv Funct Mater*,35 (24) (2025) 2423205.

22 Kamaraj M, Dodson E A & Datta S, *Adv Compos Mater*, 29 (5) (2020) 443.

23 Sarker F, Karim N, Afroj S, Koncherry V, Novoselov K S & Potluri P, *ACS Appl Mater Interfaces*, 10 (40) (2018) 34502.

24 Qin W, Vautard F, Drzal LT & Yu J, *Compos Part B Eng*,69 (2015) 335.

25 Shen X, Wang Z, Wu Y, Liu X, He Y B & Kim J K, *Nano Lett*, 16 (6) (2016) 3585.

26 Srivastava A K, Gupta V, Yerramalli C S & Singh A, *Compos Part B Eng*,179 (2019) 107539.

27 Boudjellal A, Trache D, Bekhouche S, Khimeche K, Razali MS & Guettiche D, *Mater Lett*,289 (2021) 129379.

28 Maneval L, Atawa B, Serghei A, Sintes-Zydowicz N & Beyou E, *J Mater Chem C*, 9 (40) (2021) 14247.

29 Chen J H, Cullen W G, Jang C, Fuhrer M S & Williams E D, *Phys Rev Lett*, 102 (23) (2009) 236805.

30 Ott A K & Ferrari A C, *Raman spectroscopy of graphene and related materials*, 2nd ed. ed, (Elsevier, Chakraborty, T., Ed), (2024) 233.

31 Ferrari A C, Meyer J C, Scardaci V, Casiraghi C, Lazzeri M, Mauri F, Piscanec S, Jiang D, Novoselov K S, Roth S & Geim AK, *Phys Rev Lett*, 97 (18) (2006) 187401.

32 Zahid M, Masood M T, Athanassiou A & Bayer I S, *Appl Phys Lett*, 113 (4) (2018) 044103.

33 Puchowicz D & Cieslak M, *Raman spectroscopy in the analysis of textile structures*, (intechopen), (2022).

34 Esteve-Adell I, Porcel-Valenzuela M, Zubizarreta L, Gil-Agustí M, García-Pellicer M & Quijano-Lopez A, *Front Chem*,10 (2022) 807980.

35 Dericiler K, Alishah H M, Bozar S, Güneş S & Kaya F, *Appl Phys A*, 126 (11) (2020) 904.

36 Ouadil B, Cherkaoui O, Safi M & Zahouily M, *Appl Surf Sci*,414 (2017) 292.

37 Blurton M T, Walker M, Tang F, Ladislaus P, Raine T, Degirmenci V & McNally T, *Mater Today Nano*, 28 (2024) 100518.

38 Moradkhani G, Profili J, Robert M, Laroche G & Elkoun S, *Coatings*, 13 (6) (2023) 1036.

39 Chen X, Wang X & Fang D, *Fuller Nanotubes Carbon Nanostruct*, 28 (12) (2020) 1048.

40 Alipour A, Lin R & Jayaraman K, *J Mater Res Technol*, 15 (2021) 4610.

41 Johra F T, Lee J W & Jung W G, *J Ind Eng Chem*,20 (5) (2014) 2883.

42 Ali I, Kim NK & Bhattacharyya D, *Molecules*,26 (13) (2021) 4094.

43 Kim & Lee S, *Polymers*,11 (2019) 928.

44 Chiou Y C, Olukan T, AlMahri M, Apostoleris H, Chiu C H, Lai C Y, Lu J Y, Santos S, Almansouri I & Chiesa M, *Langmuir*,34 (41)(2018) 12335.

45 Sarker F, Potluri P, Afroj S, Koncherry V, Novoselov KS & Karim N, *ACS Appl Mater Interfaces*,11 (23) (2019) 21166.